Research Square

Preprints are preliminary reports that have not undergone peer review.
They should not be considered conclusive, used to inform clinical practice,
or referenced by the media as validated information.

Refractive Axial Sensitivity Index: A Novel Metric for Quantifying the Optical Efficiency of Axial Elongation in Myopia Progression

Jiongwen Lin

Joint Shantou International Eye Centre of Shantou University and The Chinese University of Hong Kong, Shantou, Guangdong, China.

Huan Luo

Joint Shantou International Eye Centre of Shantou University and The Chinese University of Hong Kong, Shantou, Guangdong, China.

Mingzhi Zhang

zmz@jsiec.org

Joint Shantou International Eye Centre of Shantou University and The Chinese University of Hong Kong, Shantou, Guangdong, China.

Research Article

Keywords: myopia, refractive axial sensitivity index, axial length, crystalline lens compensation, anterior chamber depth

Posted Date: March 25th, 2026

DOI: https://doi.org/10.21203/rs.3.rs-8961896/v1

License: This work is licensed under a Creative Commons Attribution 4.0 International License.
Read Full License

Additional Declarations: No competing interests reported.

Abstract

Purpose

To introduce and validate the Refractive Axial Sensitivity Index (RASI), a novel metric quantifying the refractive change per unit of axial elongation, and to investigate factors influencing the optical efficiency of ocular growth in children and adolescents.

Methods

This longitudinal cohort study enrolled 13,860 children aged 6–18 years with complete biometric and cycloplegic refraction data at baseline and one-year follow-up. RASI was defined as |ΔSE/ΔAL|, where SE denotes spherical equivalent and AL denotes axial length. Multivariable linear regression and restricted cubic spline (RCS) analyses were employed to identify factors associated with RASI and the ratio of anterior chamber depth change to axial length change (ΔACD/ΔAL).

Results

The mean RASI was 2.05 D/mm. ΔACD/ΔAL emerged as the strongest independent predictor of RASI (β = 2.575, 95% CI: 2.469–2.681, P < 0.001). RASI exhibited a nonlinear relationship with axial elongation rate, peaking at 2.28 D/mm at an elongation rate of 0.27 mm/year before declining to a nadir of 1.76 D/mm at 0.59 mm/year, then rising again at rates exceeding 0.60 mm/year. Female participants demonstrated significantly higher RASI compared with males (2.17 vs. 1.94 D/mm, P = 0.033).

Conclusions

RASI provides a clinically meaningful metric for characterizing individual differences in the refractive consequences of axial elongation. The nonlinear relationship between axial elongation rate and RASI likely reflects dynamic crystalline lens compensation mechanisms, with distinct phases corresponding to physiological growth, active compensation, and compensatory exhaustion. These findings offer novel insights into the heterogeneous mechanisms underlying myopia progression.

1. INTRODUCTION

Myopia has emerged as one of the most pressing global public health challenges, with particularly high prevalence in East Asia, where school-age children in China exhibit myopia and high myopia rates of 36.6% and 5.3%, respectively [1]. High myopia, typically defined as a spherical equivalent (SE) ≤ − 6.00 diopters (D) or axial length (AL) ≥ 26 mm, represents not merely a refractive error but a pathological condition associated with multiple sight-threatening complications that may lead to irreversible vision

loss [2–4]. Consequently, elucidating the mechanisms underlying myopia onset and progression is of paramount importance for developing effective prevention and control strategies.

Current clinical monitoring of myopia progression primarily relies on absolute changes in SE and AL [5]. In the standard simplified schematic eye model, each millimeter of axial elongation typically corresponds to approximately − 2.5 to − 3.0 D of myopic shift [6]. However, substantial inter-individual variability exists in the relationship between axial elongation and refractive change [7]: some children exhibit rapid axial growth with relatively modest refractive progression, whereas others demonstrate significant myopic shift despite minimal axial elongation. This heterogeneity in the AL–refraction relationship suggests that the "optical efficiency" of ocular growth varies considerably among individuals, yet the determinants and underlying mechanisms remain inadequately characterized. Therefore, there is an urgent need to establish a metric capable of quantifying "the refractive change corresponding to each unit of axial elongation" to more precisely reflect the optical efficiency of ocular growth.

The present study introduces a novel quantitative metric—the Refractive Axial Sensitivity Index (RASI)—defined as the absolute value of the ratio of SE change to AL change (|ΔSE/ΔAL|), which captures the net outcome of all compensatory and pathological processes. Although modern optical biometry enables precise measurement of individual ocular components, including AL, anterior chamber depth (ACD), lens thickness (LT), and corneal curvature (K) [8], SE can theoretically be calculated from these biometric parameters using established optical equations [9]. In an incompletely observable ocular development system where not all determinants can be accurately measured or modeled, RASI serves as a practical indicator of growth–refraction conversion efficiency, integrating both known and unknown factors influencing refractive development. Additionally, this study introduces the ratio of ACD change to AL change (ΔACD/ΔAL) to explore the influence of anterior segment structural changes on refractive sensitivity. These metrics are anticipated to provide novel perspectives for understanding individual differences in myopia progression and establishing a theoretical foundation for precision myopia management strategies.

2. METHODS

2.1 Study Design and Participants

This longitudinal cohort study was designed to investigate the relationship between AL elongation and SE change over a one-year follow-up period in children and adolescents. Participants were recruited from the Joint Shantou International Eye Center of Shantou University and The Chinese University of Hong Kong (JSIEC) between 2020 and 2025. The study protocol adhered to the principles of the Declaration of Helsinki and was approved by the institutional ethics committee. Written informed consent was obtained from all participants and their legal guardians prior to enrollment.

Inclusion criteria comprised: (1) age 6–18 years at baseline examination; (2) complete ocular biometric data at both baseline and follow-up; (3) cycloplegic refraction meeting quality control standards at both

visits; and (4) follow-up interval of 9–15 months.

Exclusion criteria included: (1) history of intraocular surgery or ocular trauma; (2) ocular diseases potentially affecting refractive development, such as congenital cataract, keratoconus, and glaucoma; (3) strabismus or amblyopia that may influence refractive progression; and (4) current or prior use of any myopia control interventions, including orthokeratology, low-dose atropine, or peripheral defocus lenses.

2.2 Ocular Biometry and Refraction

Comprehensive ocular biometry was performed using an optical biometer (Tomey OA2000, Japan). Measured parameters included: AL, ACD, central corneal thickness (CCT), LT, white-to-white corneal diameter (WTW), and pupil diameter. Corneal curvature was measured along the two principal meridians to obtain flat keratometry (K1) and steep keratometry (K2); mean keratometry (Km) was calculated as the arithmetic mean of K1 and K2.

Cycloplegic refraction was performed 30 minutes after instillation of 1% cyclopentolate hydrochloride eye drops (administered twice at 5-minute intervals). Adequate cycloplegia was confirmed by pupil diameter ≥ 6 mm and absence of light reflex. Refractive measurements were obtained using an autorefractor (KR-800; Topcon Corporation, Tokyo, Japan), with subjective refinement performed when necessary. SE was calculated as: sphere power + (cylinder power/2).

All measurements were conducted by experienced ophthalmic technicians following standardized protocols. To avoid statistical bias arising from inter-eye correlation, only right eye data were included in all analyses.

2.3 Variable Definitions

2.3.1 Primary Outcome Variable

The primary outcome variable was RASI, defined as the absolute value of the ratio of SE change to AL change:

$$RASI = |\Delta SE/\Delta AL| \ (D/mm)$$

where $\Delta SE = SE_{follow\text{-}up} - SE_{baseline}$ and $\Delta AL = AL_{follow\text{-}up} - AL_{baseline}$. This index quantifies the refractive change corresponding to each unit of axial elongation, reflecting the optical efficiency of ocular growth.

2.3.2 Secondary Outcome Variables

Secondary outcome variables included ΔACD/ΔAL and change in lens thickness ($\Delta LT = LT_{follow\text{-}up} - LT_{baseline}$). ΔACD/ΔAL was calculated as:

$$\Delta ACD/\Delta AL = (ACD_{follow\text{-}up} - ACD_{baseline})/\Delta AL$$

This ratio reflects the relative contribution of anterior segment structural changes to overall axial elongation.

2.3.3 Covariate Classification

Refractive status was classified into five groups based on baseline SE: (1) high hyperopia (SE ≥ + 5.00 D); (2) low-to-moderate hyperopia (+ 0.50 D ≤ SE < + 5.00 D); (3) emmetropia (− 0.50 D < SE < + 0.50 D); (4) low-to-moderate myopia (− 6.00 D < SE ≤ − 0.50 D); and (5) high myopia (SE ≤ − 6.00 D). Age groups were defined according to developmental stages: (1) early school age (6–9 years); (2) middle school age (10–12 years); (3) adolescence (13–15 years); and (4) late adolescence (16–18 years). For axial elongation rate classification, ΔAL was annualized based on the follow-up interval, and participants were categorized into three groups: (1) slow elongation (≤ 0.20 mm/year); (2) moderate elongation (0.20–0.40 mm/year); and (3) rapid elongation (≥ 0.40 mm/year).

2.4 Statistical Analysis

2.4.1 Descriptive Statistics

Continuous variables were expressed as mean ± standard deviation (SD) or median (interquartile range, IQR) based on the results of Shapiro–Wilk normality tests. Categorical variables were presented as frequencies and percentages. Baseline characteristics across refractive status groups were compared using one-way analysis of variance (ANOVA) or Kruskal–Wallis tests for continuous variables and chi-square tests for categorical variables.

2.4.2 Subgroup Comparisons

Differences in RASI and ΔACD/ΔAL across subgroups were compared. One-way ANOVA with Bonferroni correction for multiple comparisons was employed for comparisons among age groups and axial elongation rate groups. Sex differences were assessed using independent samples t-tests or Mann–Whitney U tests.

2.4.3 Multivariable Linear Regression Analysis

Prior to multivariable linear regression analysis, all continuous independent variables were Z-score standardized to identify factors independently associated with RASI. Two hierarchical models were constructed:

Model 1 (Basic Model)

Included age, sex, and baseline AL for regression analysis of both RASI and ΔACD/ΔAL.

Model 2 (Full Model)

Extended Model 1 by incorporating variables related to baseline refractive media, including ACD, LT, Km, and CCT.

2.4.4 Assessment of Nonlinear Relationships

Given the potential nonlinear relationships between continuous predictors and RASI or ΔACD/ΔAL, restricted cubic spline (RCS) analyses were conducted within the multivariable regression framework (Model 2). Spline functions were constructed with four knots located at the 5th, 35th, 65th, and 95th percentiles of each predictor distribution. Analyses examined relationships between RASI and ΔACD/ΔAL, as well as between axial elongation rate and both RASI and ΔACD/ΔAL.

2.4.5 Missing Data Handling

Following confirmation of the missing completely at random (MCAR) assumption via Little's MCAR test, mean imputation was applied to missing continuous baseline variables. Complete case analysis was performed as a sensitivity analysis.

2.4.6 Statistical Software

All statistical analyses were performed using R software (version 4.3.0; R Foundation for Statistical Computing, Vienna, Austria). RCS analyses were conducted using the "rms" package, data visualization using the "ggplot2" package, and correlation matrix heatmaps using the "corrplot" package. All statistical tests were two-sided, with $P < 0.05$ considered statistically significant.

3. RESULTS

3.1 Baseline Characteristics

A total of 13,860 children and adolescents were enrolled, with a mean age of 12.47 ± 2.67 years and an overall mean RASI of 2.05 D/mm. Baseline characteristics differed significantly across refractive status groups (all $P < 0.05$) (Table 1). The high myopia group exhibited the highest mean age (13.10 ± 2.83 years). Baseline AL increased progressively with myopia severity, with ACD demonstrating a similar trend, whereas LT exhibited an inverse relationship. During follow-up, the emmetropia and low-to-moderate myopia groups showed the greatest axial elongation.

Table 1
Baseline characteristics of study participants stratified by refractive status

Variables	High Hyperopia	Low-Moderate Hyperopia	Emmetropia	Low-Moderate Myopia	High Myopia	P value
	(SE ≥ + 5.00 D)	(+ 0.50 ≤ SE < + 5.00 D)	(− 0.50 < SE < + 0.50 D)	(− 6.00 < SE ≤ − 0.50 D)	(SE ≤ − 6.00 D)	
n (%)	549 (4.0)	3,079 (22.2)	1,816 (13.1)	7,389 (53.3)	1,027 (7.4)	
Age (years)	11.28 ± 2.49	10.66 ± 2.63	11.33 ± 2.55	12.85 ± 2.52	13.10 ± 2.83	**< 0.001**
Male, n (%)	326 (59.4)	1,571 (51.0)	930 (51.2)	3,850 (52.1)	536 (52.2)	**0.009**
Baseline ocular biometry						
AL (mm)	20.88 ± 0.86	22.44 ± 0.81	23.33 ± 0.79	24.40 ± 0.93	26.64 ± 1.32	**< 0.001**
ACD (mm)	3.40 ± 0.25	3.48 ± 0.23	3.63 ± 0.25	3.74 ± 0.22	3.72 ± 0.25	**< 0.001**
CCT (μm)	540.37 ± 26.12	534.38 ± 27.68	533.73 ± 27.14	535.80 ± 27.28	532.92 ± 29.21	**< 0.001**
K1 (D)	42.20 ± 1.39	42.55 ± 1.35	42.73 ± 1.28	42.83 ± 1.21	42.66 ± 1.34	**< 0.001**
K2 (D)	44.15 ± 1.38	44.49 ± 1.54	44.45 ± 1.51	44.43 ± 1.40	44.73 ± 1.58	**< 0.001**
LT (mm)	3.57 ± 0.19	3.54 ± 0.15	3.48 ± 0.15	3.43 ± 0.14	3.46 ± 0.15	**< 0.001**
WTW (mm)	11.97 ± 0.43	11.98 ± 0.44	12.00 ± 0.43	12.01 ± 0.43	11.98 ± 0.48	**0.009**
Pupil diameter (mm)	7.25 ± 0.97	7.32 ± 0.91	7.41 ± 0.86	7.42 ± 0.92	7.47 ± 0.92	**< 0.001**
SE (D)	6.72 ± 1.42	1.80 ± 1.18	−0.01 ± 0.23	−2.37 ± 1.39	−8.77 ± 2.77	**< 0.001**
BCVA (decimal)	0.70 ± 0.22	0.84 ± 0.18	0.91 ± 0.17	0.92 ± 0.14	0.75 ± 0.21	**< 0.001**
Changes during follow-up						
ΔSE (D)	0.59 ± 0.51	0.50 ± 0.43	0.79 ± 0.58	0.82 ± 0.51	0.58 ± 0.45	**< 0.001**

Variables	High Hyperopia	Low-Moderate Hyperopia	Emmetropia	Low-Moderate Myopia	High Myopia	P value
	(SE ≥ + 5.00 D)	(+ 0.50 ≤ SE < + 5.00 D)	(− 0.50 < SE < + 0.50 D)	(− 6.00 < SE ≤ − 0.50 D)	(SE ≤ − 6.00 D)	
ΔAL (mm)	0.26 ± 0.19	0.27 ± 0.18	0.42 ± 0.23	0.40 ± 0.21	0.26 ± 0.17	**< 0.001**
ΔACD (mm)	0.11 ± 0.11	0.09 ± 0.11	0.09 ± 0.12	0.06 ± 0.07	0.05 ± 0.05	**< 0.001**
ΔLEN (mm)	-0.05 ± 0.20	-0.04 ± 0.14	-0.04 ± 0.11	-0.02 ± 0.12	-0.01 ± 0.11	**< 0.001**
Outcome measures						
RASI (D/mm)	2.20 ± 5.82	2.20 ± 4.48	2.10 ± 3.28	1.95 ± 8.42	2.16 ± 3.93	**< 0.001**
ΔACD/ΔAL	0.61 ± 1.59	0.47 ± 1.28	0.30 ± 0.85	0.18 ± 0.67	0.25 ± 0.94	**< 0.001**
Age group, n (%)						**< 0.001**
Early school age (6–9 years)	75 (13.7)	738 (24.0)	249 (13.7)	315 (4.3)	59 (5.7)	
Middle school age (10–12 years)	242 (44.1)	1,241 (40.3)	749 (41.2)	1,958 (26.5)	250 (24.3)	
Adolescence (13–15 years)	170 (31.0)	846 (27.5)	601 (33.1)	3,124 (42.3)	369 (35.9)	
Late adolescence (16–18 years)	62 (11.3)	254 (8.2)	217 (11.9)	1,992 (27.0)	349 (34.0)	
Axial elongation rate, n (%)						**< 0.001**
Slow (≤ 0.20 mm/year)	235 (42.8)	1,161 (37.7)	282 (15.5)	1,052 (14.2)	344 (33.5)	
Moderate (0.20–0.40 mm/year)	181 (33.0)	1,266 (41.1)	570 (31.4)	2,619 (35.4)	428 (41.7)	
Rapid (≥ 0.40 mm/year)	133 (24.2)	652 (21.2)	964 (53.1)	3,718 (50.3)	255 (24.8)	

Abbreviations: AL, axial length; ACD, anterior chamber depth; CCT, central corneal thickness; K1, flat keratometry; K2, steep keratometry; LT, lens thickness; WTW, white-to-white corneal diameter; SE, spherical equivalent; BCVA, best-corrected visual acuity; RASI, refractive axial sensitivity index.

Continuous variables are presented as mean ± SD. Categorical variables are presented as n (%). P values were calculated using one-way ANOVA or Kruskal-Wallis test for continuous variables and chi-square test for categorical variables.

The primary outcome, RASI, differed significantly across refractive status groups ($P < 0.05$), with the low-to-moderate myopia group demonstrating the lowest RASI (1.95 ± 8.42 D/mm). ΔACD/ΔAL decreased progressively with increasing myopia severity, being highest in the high hyperopia group (0.61 ± 1.59) and lowest in the low-to-moderate myopia group (0.18 ± 0.67).

3.2 RASI and ΔACD/ΔAL Across Subgroups

RASI differed significantly across age groups ($P = 0.002$). RASI increased progressively with age: early school age (6–9 years): 1.74 D/mm; middle school age (10–12 years): 1.96 D/mm; adolescence (13–15 years): 1.99 D/mm; and late adolescence (16–18 years): 2.46 D/mm (Fig. 1A). ΔACD/ΔAL did not differ significantly across age groups (Fig. 1B).

RASI also differed significantly between sexes ($P = 0.033$), with females demonstrating significantly higher RASI than males (2.17 vs. 1.94 D/mm) (Fig. 1C). ΔACD/ΔAL did not differ significantly between sexes (Fig. 1D).

Both RASI and ΔACD/ΔAL differed significantly across axial elongation rate groups ($P < 0.05$). The slow elongation group (≤ 0.20 mm/year) exhibited the highest RASI (2.43 D/mm) and ΔACD/ΔAL (0.59) (Figs. 1E and 1F).

3.3 Multivariable Regression Analysis

Complete results of multivariable linear regression analyses for RASI and ΔACD/ΔAL are presented in Supplementary Table 1; only variables with $P < 0.05$ are shown in the visualizations.

Multivariable linear regression results for RASI are presented in Table 2. ΔACD/ΔAL emerged as the strongest independent predictor of RASI. After adjustment for sex, age, and refractive media parameters, ΔACD/ΔAL remained significantly positively associated with RASI ($\beta = 2.575$, 95% CI: 2.469–2.681, $P < 0.001$), indicating that a higher proportion of ACD change relative to total axial change was associated with greater refractive change per unit of axial elongation. Age was independently and positively associated with RASI, with the effect size increasing in Model 2 (Model 1: $\beta = 0.206$, $P < 0.001$; Model 2: $\beta = 0.321$, $P < 0.001$). Baseline AL was negatively associated with RASI (Model 2: $\beta = -0.196$, $P = 0.010$). Axial elongation rate was significantly negatively associated with RASI. Compared with the slow elongation group, both the moderate elongation group (Model 2: $\beta = -0.423$, $P = 0.007$) and rapid elongation group (Model 2: $\beta = -0.313$, $P = 0.046$) demonstrated significantly lower RASI, suggesting that individuals with rapid axial growth exhibit smaller refractive changes per millimeter of elongation.

Multivariable analysis with ΔACD/ΔAL as the dependent variable revealed determinants of the proportion of ACD change (Table 3). Baseline AL was among the strongest negative predictors (Model 2: β = −0.101, P < 0.001). Axial elongation rate demonstrated a dose–response negative relationship with ΔACD/ΔAL: compared with the slow elongation group, both moderate and rapid elongation groups showed significantly lower ΔACD/ΔAL, with larger effect sizes in the rapid elongation group. Additionally, baseline LT and baseline WTW were significantly positively associated with ΔACD/ΔAL, whereas baseline ACD and baseline pupil diameter were negatively associated.

Variance inflation factor (VIF) analysis for Model 2 (Supplementary Table 2) revealed all VIF values < 5, indicating no substantial multicollinearity.

3.4 Restricted Cubic Spline Analysis

RCS analyses were employed to assess potential nonlinear relationships between continuous predictors and RASI or ΔACD/ΔAL. All analyses were conducted within the Model 2 framework, and results are summarized in Fig. 2.

3.4.1 Nonlinear Relationships with RASI

After adjustment for sex, age, and refractive media parameters, ΔACD/ΔAL demonstrated a significant positive association with RASI (Fig. 2A). RASI exhibited a continuous upward trend with increasing ΔACD/ΔAL. This finding reveals a close relationship between the pattern of ACD change and refractive sensitivity: a greater proportion of ACD change within axial elongation is associated with more pronounced refractive change per unit of axial elongation.

The spline curve for axial elongation rate versus RASI (Fig. 2B) demonstrated that at lower axial growth rates, RASI increased with increasing growth rate, reaching a predicted maximum of 2.28 D/mm at an elongation rate of 0.27 mm/year. Beyond this threshold, RASI declined. Notably, when axial growth rate exceeded approximately 0.6 mm/year, the relationship reversed, with RASI rising again with further increases in elongation rate.

3.4.2 Nonlinear Relationships with ΔACD/ΔAL

A significant nonlinear relationship existed between baseline AL and ΔACD/ΔAL (Pnonlinearity < 0.001) (Fig. 2C), with the spline curve exhibiting a U-shaped distribution. When baseline AL < 25.49 mm, ΔACD/ΔAL values were higher, indicating that ACD changes accounted for a larger proportion of total axial elongation in these eyes. As AL increased, ΔACD/ΔAL declined rapidly, reaching a nadir (approximately − 0.1) at AL = 25.49 mm, before stabilizing or slightly increasing. This nonlinear relationship suggests that growth in shorter eyes involves greater anterior segment structural changes, whereas growth in longer eyes predominantly manifests as posterior segment elongation.

Additionally, a nonlinear relationship was observed between axial elongation rate and ΔACD/ΔAL (Fig. 2D). The spline curve demonstrated that during the initial phase of increasing axial growth rate, the

proportion of anterior chamber deepening in total axial elongation declined rapidly, reaching a nadir (ΔACD/ΔAL = 0.152) at an elongation rate of 0.68 mm/year. Beyond this inflection point, ΔACD/ΔAL exhibited a gradual upward trend with further increases in axial elongation rate.

3.4.3 Nonlinear Relationships with ΔLT

RCS analysis of the ΔLT model within the Model 2 framework was also performed (Supplementary Fig. 1). A negative correlation existed between ΔACD/ΔAL and ΔLT (Supplementary Fig. 1A). As ΔACD/ΔAL increased, ΔLT exhibited a gradual declining trend. The spline curve for axial elongation rate versus ΔLT (Supplementary Fig. 1B) demonstrated that during the low axial growth rate phase (< 0.27 mm/year), ΔLT remained at relatively low levels (approximately − 0.015 to − 0.020 mm), with a relatively flat curve and low sensitivity to changes in growth rate. When axial growth rate exceeded 0.27 mm/year, the curve slope increased sharply, with ΔLT declining precipitously from approximately − 0.020 mm to approximately − 0.050 mm. When axial growth rate exceeded approximately 0.6 mm/year, the curve flattened.

3.5 Sensitivity Analyses

Three sensitivity analyses were conducted to demonstrate the robustness of the main findings (Supplementary Table 3): (1) the positive association between ΔACD/ΔAL and RASI remained significant after exclusion of samples with minimal ΔAL; (2) the nonlinear inflection points for axial growth rate remained stable after bootstrap validation and piecewise regression, with 95% confidence intervals encompassing the primary analysis estimates; and (3) in complete case analysis, the direction and significance of core regression results remained consistent with imputed data, indicating that missing data handling methods did not substantially influence the main conclusions.

4. DISCUSSION

The ratio of ACD change to AL change (ΔACD/ΔAL) emerged as the strongest independent predictor of refractive sensitivity (RASI) in multivariable analysis (positive correlation), a relationship that was confirmed by RCS analysis. This indicates that the greater the contribution of the anterior chamber to axial elongation, the larger the refractive change induced by each millimeter of axial growth. According to Gaussian optical analysis based on the Gullstrand schematic eye model by Chang et al. [10], each millimeter increase in ACD produces + 1.35 D of hyperopic shift, whereas each millimeter increase in vitreous chamber depth (VCD) produces − 2.67 D of myopic shift—seemingly contradicting the principle that "greater ΔACD/ΔAL is associated with more pronounced refractive change."

According to the dynamic optical model study published by Jóźwik et al. [11] in the Journal of Vision, the eye functions as a two-lens system (cornea + crystalline lens), with total refractive power following the Gullstrand equation:

$$P_{total} = P_{cornea} + P_{lens} - (d \times P_{cornea} \times P_{lens})/n$$

where d represents the distance between the principal planes of the two refractive elements, closely related to ACD. This implies that when ACD increases, total system power increases, directly participating in the reconfiguration of system refractive power. In contrast, when VCD increases, it merely changes the distance between the focal plane and the retina. The nodal point of the eye is located within the crystalline lens (approximately 7.08–7.33 mm from the cornea), and rays passing through the nodal point have equal incident and emergent angles, which is crucial for retinal image formation [12].

When ACD changes, the principal plane separation of the compound system changes. According to the analysis by Evans and Harris [13], principal plane positions determine the equivalent focal length of the system. ACD changes lead to repositioning of these critical optical reference points, thereby affecting the refractive properties of the entire system. This "optical lever" effect of the anterior chamber explains why the same amount of axial elongation produces different refractive effects depending on location. On the other hand, the crystalline lens effectively compensates for myopic shift induced by axial elongation through reduction in refractive power [14]. Emmetropic children exhibit only approximately 0.05 D refractive change per millimeter of axial growth (effective compensation), with the lens continuing to thin until age 9–10 years [15–17]. In contrast, myopic children exhibit 1.0–1.4 D refractive change per millimeter of axial growth (insufficient compensation) [18]. Rozema et al. [19] identified a critical temporal feature: pre-myopic children exhibited higher rates of lens power loss (− 0.71 D/year vs. −0.46 D/year in emmetropes) before myopia onset, but this compensation slowed after myopia development. The present study revealed a negative correlation between this lens thinning process and ACD deepening, suggesting that high ΔACD/ΔAL may reflect an "exhausted" state of the lens compensation mechanism, with increased net refractive effect per unit of axial growth. This also explains why the refractive "cost" per unit of axial growth increases with age or axial length in the present study.

Jones et al. [20] demonstrated that in emmetropic children, axial growth rate gradually declines from approximately 0.20 mm/year at age 6 to below 0.10 mm/year by age 14, with axial growth during this period primarily representing normal developmental growth. The present study found that during the low axial growth rate phase (< 0.27 mm/year), ΔACD/ΔAL remained at relatively high levels within this range (approximately 0.6), indicating that ACD change accounts for a large proportion of total axial change. Wong et al. [21] reported in the Singapore children's cohort study that ACD in emmetropic children continues to deepen until age 9–10 years, driven by equatorial expansion of the crystalline lens and developmental remodeling of the zonular-ciliary body complex rather than pathological remodeling of the posterior sclera [22]. The present study found that lens thinning magnitude during this phase was minimal and the curve was flat, with low sensitivity to changes in growth rate. It has been reported that prior to myopia onset, lens thinning rates are similar between future myopes and emmetropes [23], as the axial growth rate itself remains on a "normal trajectory," with compensation mechanisms either not triggered or in low demand. Additionally, this change is independent of axial growth rate, with RASI increasing as growth rate increases (from approximately 1.2 D/mm to a peak of 2.276 D/mm).

When axial growth rate exceeds 0.27 mm/year, the slope of the ΔLT RCS curve increases sharply, with lens thinning magnitude accelerating from approximately − 0.015 mm to approximately − 0.045 mm and

becoming highly sensitive to growth rate, indicating activation of the lens compensation mechanism attempting to compensate for myopic shift from posterior segment elongation through power reduction. During this period, axial growth pattern undergoes a fundamental shift from "balanced anterior-posterior" to "posterior-dominant," with ΔACD/ΔAL declining sharply to a nadir of 0.15 (corresponding to growth rate 0.68 mm/year). Saw et al. [24] conducted a three-year follow-up study: myopic children exhibited 0.89 mm axial elongation, of which ACD changed by only − 0.02 mm while VCD increased by 0.92 mm—nearly equal to the total elongation. In the 0.27–0.59 mm/year range, RASI declined from a peak of 2.276 D/mm to a nadir of 1.760 D/mm. This decline similarly reflects the gradual emergence of lens compensatory effects. Although lens thinning is more pronounced during this period, ΔACD/ΔAL declines. This apparent paradox actually reflects a critical fact: while lens thinning should theoretically lead to anterior chamber deepening, during the moderate growth phase, selective remodeling of the posterior sclera causes VCD elongation rate to far exceed ACD deepening rate, resulting in decreased ΔACD/ΔAL ratio. In other words, the "spatial dividend" from lens thinning is "diluted" by posterior segment elongation.

RCS plots demonstrated that when axial growth rate exceeds approximately 0.6–0.7 mm/year, the ΔLT curve flattens, with lens thinning magnitude remaining at approximately − 0.050 to − 0.055 mm and becoming insensitive to further increases in growth rate, suggesting that the compensation mechanism has reached its biological limit [23, 25]. RASI rises again, with each millimeter of axial growth almost entirely converting to myopic shift. This statistical evidence directly confirms the "exhausted" state of lens compensation in rapidly progressive myopia. This "compensation interruption" may originate from anatomical space constraints [26] and biomechanical tolerance of the crystalline lens. The present study found that when axial growth rate exceeds the nadir point of 0.68 mm/year, ΔACD/ΔAL begins to gradually recover. Spherical structures exhibit uniform stress distribution at all points under the same pressure, with intraocular pressure producing more uniform expansion effects on the weakened global scleral wall, including the usually protected equatorial and anterior scleral regions beginning to yield [27].

The present study also found that RASI was significantly higher in females than in males (2.17 vs. 1.94 D/mm), potentially related to females' shorter mean axial length (approximately 0.5 mm) [28, 29] and earlier pubertal development, causing female ocular optical components to reach their compensation limits earlier [30, 31].

This study has several strengths. First, the large sample (N = 13,860) spans a broad age range. Second, standardized ocular biometry and cycloplegic refraction methods were employed. However, as a single-center study with predominantly Chinese Han participants, the generalizability of findings to other ethnic populations requires further validation. Additionally, the one-year follow-up period may be insufficient to fully capture the long-term dynamics of RASI. Future research should incorporate longer follow-up periods and multi-ethnic cohorts to further elucidate the biological mechanisms and clinical utility of RASI.

5. CONCLUSION

This study, utilizing large-scale longitudinal cohort data, represents the first systematic characterization of the distribution and determinants of the Refractive Axial Sensitivity Index (RASI) in children and adolescents. RASI was found to increase with age, be higher in females than males, and paradoxically lower in rapid axial elongators. The nonlinear relationship between axial elongation rate and RASI likely reflects dynamic crystalline lens compensation mechanisms, with distinct phases corresponding to physiological growth, active compensation, and compensatory exhaustion. These findings provide novel insights into individual differences in myopia development and establish a theoretical foundation for precision myopia management strategies.

Declarations

1. Consent to Publish declaration: not applicable.

2. Ethics and Consent to Publish declarations: not applicable.

Funding source:

This work was supported by grants from the National Natural Science Foundation of P.R. China (Grant No. 82471124)

Author Contribution

J.L. wrote the main manuscript text, and H.L. processed the data. All authors reviewed the manuscript.

References

1. Pan W, Saw SM, Wong TY, Morgan I, Yang Z, Lan W. Prevalence and temporal trends in myopia and high myopia children in China: a systematic review and meta-analysis with projections from 2020 to 2050. Lancet Reg Health West Pac. 2025;55:101484. Published 2025 Jan 27. doi:10.1016/j.lanwpc.2025.101484
2. Du Y, Meng J, He W, Qi J, Lu Y, Zhu X. Complications of high myopia: An update from clinical manifestations to underlying mechanisms. Adv Ophthalmol Pract Res. 2024;4(3):156-163. Published 2024 Jun 21. doi:10.1016/j.aopr.2024.06.003
3. Shah R, Vlasak N, Evans BJW. High myopia: Reviews of myopia control strategies and myopia complications. Ophthalmic Physiol Opt. 2024;44(6):1248-1260. doi:10.1111/opo.13366
4. Haarman AEG, Enthoven CA, Tideman JWL, Tedja MS, Verhoeven VJM, Klaver CCW. The Complications of Myopia: A Review and Meta-Analysis. Invest Ophthalmol Vis Sci. 2020;61(4):49. doi:10.1167/iovs.61.4.49
5. Ohlendorf A, Sankaridurg P. Turbocharge myopia management with axial length measurement. Review of Myopia Management. 2024.

6. Brennan NA, Toubouti YM, Cheng X, Bullimore MA. Efficacy in myopia control. Prog Retin Eye Res. 2021;83:100923. doi:10.1016/j.preteyeres.2020.100923
7. Cruickshank FE, Logan NS. Optical 'dampening' of the refractive error to axial length ratio: implications for outcome measures in myopia control studies. Ophthalmic Physiol Opt. 2018;38(3):290-297. doi:10.1111/opo.12457
8. Bullimore MA, Slade S, Yoo P, Otani T. An Evaluation of the IOLMaster 700. Eye Contact Lens. 2019;45(2):117-123. doi:10.1097/ICL.0000000000000552
9. Morgan PB, McCullough SJ, Saunders KJ. Estimation of ocular axial length from conventional optometric measures. Cont Lens Anterior Eye. 2020;43(1):18-20. doi:10.1016/j.clae.2019.11.005
10. Chang SW, Tsai IL, Hu FR, Lin LL, Shih YF. Human eye ocular component analysis for refractive state and refractive surgery. Int J Ophthalmol. 2017;10(7):1057-1062. doi:10.18240/ijo.2017.07.06
11. Jóźwik A, Siedlecki D, Zając M. How a dynamic optical system maintains image quality: self-adjustment of the human eye. J Vis. 2021;21(3):12. doi:10.1167/jov.21.3.12
12. Atchison DA, Smith G. Optics of the Human Eye. Oxford: Butterworth-Heinemann; 2000.
13. Evans BJ, Harris CM. Paraxial schematic eyes and related calculations. Ophthalmic Physiol Opt. 2017;37(3):233-245. doi:10.1111/opo.12366
14. Mutti DO, Sinnott LT, Brennan NA, et al. The contribution of crystalline lens power to refractive error in childhood. Optom Vis Sci. 2023;100(6):360-370. doi:10.1097/OPX.0000000000002027
15. Wong HB, Machin D, Tan SB, Wong TY, Saw SM. Ocular component growth curves among Singaporean children with different refractive error status. Invest Ophthalmol Vis Sci. 2010;51(3):1341-1347. doi:10.1167/iovs.09-3431
16. Mutti DO, Mitchell GL, Jones LA, et al. Axial growth and changes in lenticular and corneal power during emmetropization in infants. Invest Ophthalmol Vis Sci. 2005;46(9):3074-3080. doi:10.1167/iovs.04-1040
17. Zadnik K, Mutti DO, Fusaro RE, Adams AJ. Longitudinal evidence of crystalline lens thinning in children. Invest Ophthalmol Vis Sci. 1995;36(8):1581-1587.
18. Chen Y, Drobe B, Zhang C, et al. Refractive change per axial length elongation among children and adolescents. Ophthalmology. 2021;128(12):1812-1814. doi:10.1016/j.ophtha.2021.06.025
19. Rozema JJ, Dankert S, Engelen S, Verbruggen KHM, Ní Dhubhghaill S. Axial length and lens power in emmetropes, low and high myopes. Ophthalmic Physiol Opt. 2019;39(4):237-247. doi:10.1111/opo.12621
20. Jones LA, Mitchell GL, Mutti DO, Hayes JR, Moeschberger ML, Zadnik K. Comparison of ocular component growth curves among refractive error groups in children. Invest Ophthalmol Vis Sci. 2005;46(7):2317-2327. doi:10.1167/iovs.04-0945
21. Wong HB, Machin D, Tan SB, Wong TY, Saw SM. Ocular component growth curves among Singaporean children with different refractive error status. Invest Ophthalmol Vis Sci. 2010;51(3):1341-1347. doi:10.1167/iovs.09-3431

22. Atchison DA, Jones CE, Schmid KL, et al. Eye shape in emmetropia and myopia. Invest Ophthalmol Vis Sci. 2004;45(10):3380-3386. doi:10.1167/iovs.04-0292
23. Mutti DO, Mitchell GL, Sinnott LT, et al. Corneal and crystalline lens dimensions before and after myopia onset. Optom Vis Sci. 2012;89(3):251-262. doi:10.1097/OPX.0b013e3182418213
24. Saw SM, Chua WH, Gazzard G, Koh D, Tan DT, Stone RA. Eye growth changes in myopic children in Singapore. Br J Ophthalmol. 2005;89(11):1489-1494. doi:10.1136/bjo.2005.071118
25. Xiong S, Sankaridurg P, Naduvilath T, et al. Longitudinal changes in lens power in Chinese children with onset of myopia. Acta Ophthalmol. 2021;99(8):e1422-e1429. doi:10.1111/aos.14855
26. Mutti DO, Zadnik K, Adams AJ. Myopia: the nature versus nurture debate goes on. Invest Ophthalmol Vis Sci. 1996;37(6):952-957.
27. McBrien NA, Gentle A. Role of the sclera in the development and pathological complications of myopia. Prog Retin Eye Res. 2003;22(3):307-338. doi:10.1016/S1350-9462(02)00063-0
28. Naduvilath T, He X, Saunders K, et al. Age, gender and regional/ethnic variations in emmetropic axial growth rate. Ophthalmic Physiol Opt. 2025;45(6):1485-1495. doi:10.1111/opo.13545
29. Cruickshank FE, Logan NS. Optical 'dampening' of the refractive error to axial length ratio: implications for outcome measures in myopia control studies. Ophthalmic Physiol Opt. 2018;38(3):290-297. doi:10.1111/opo.12457
30. McCullough S, Adamson G, Breslin KMM, McClelland JF, Doyle L, Saunders KJ. Axial growth and refractive change in white European children and young adults: predictive factors for myopia. Sci Rep. 2020;10(1):15189. Published 2020 Sep 16. doi:10.1038/s41598-020-72240-y
31. Lee SS, Mackey DA. Prevalence and Risk Factors of Myopia in Young Adults: Review of Findings From the Raine Study. Front Public Health. 2022;10:861044. Published 2022 Apr 27. doi:10.3389/fpubh.2022.861044

Tables

Tables 2 and 3 are available in the Supplementary Files section.

Figures

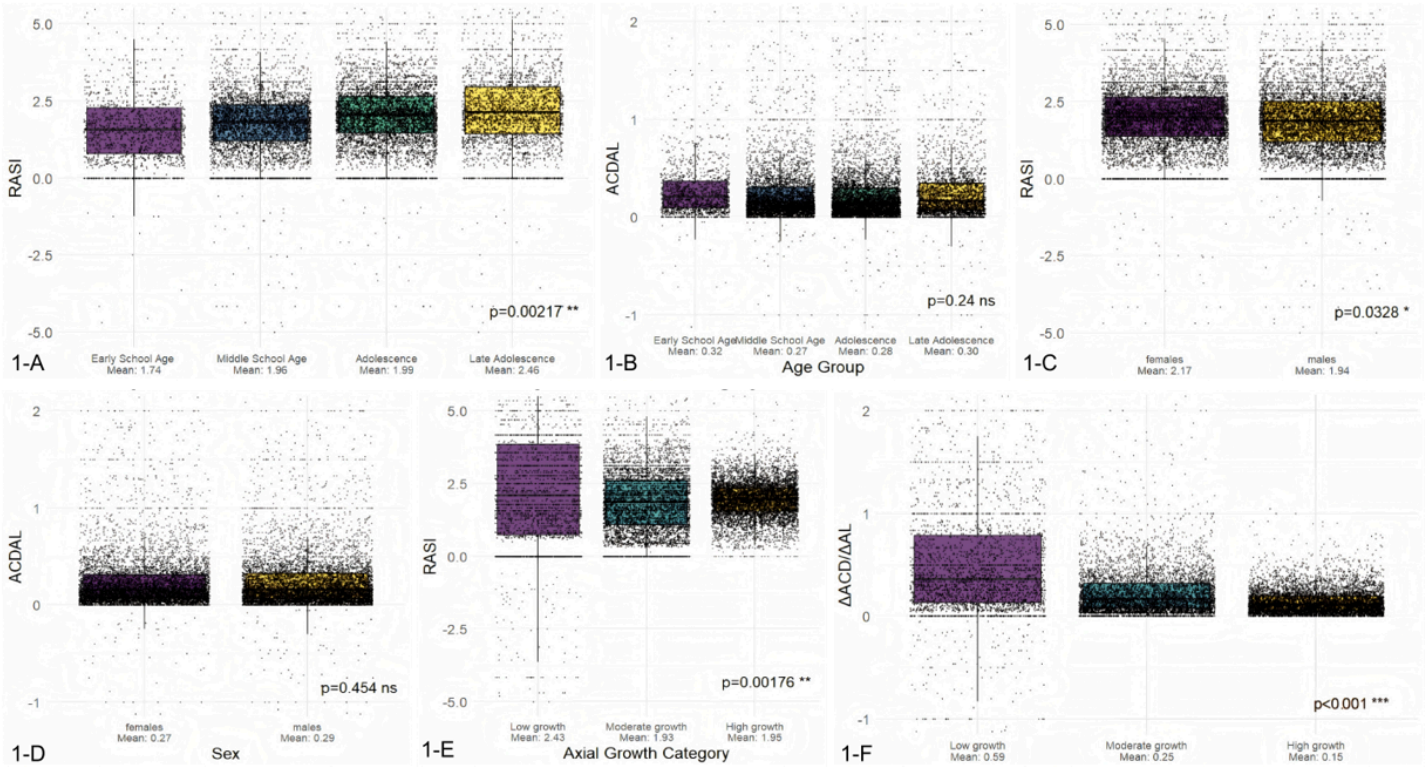


Figure 1

Distribution of RASI and ΔACD/ΔAL across demographic and clinical subgroups.

(A) RASI distribution across age groups. **(B)** ΔACD/ΔAL distribution across age groups. **(C)** RASI distribution by sex. **(D)** ΔACD/ΔAL distribution by sex. **(E)** RASI distribution across axial growth categories. **(F)** ΔACD/ΔAL distribution across axial growth categories.

Abbreviations: RASI, Refractive Axial Sensitivity Index; ΔACD/ΔAL, ratio of anterior chamber depth change to axial length change.

*P < 0.05, **P < 0.01, ***P < 0.001, ns = not significant. *Age groups:* Early School Age (6–9 years), Middle School Age (10–12 years), Adolescence (13–15 years), Late Adolescence (16–18 years). *Axial growth categories:* Low growth (≤0.20 mm/year), Moderate growth (0.20–0.40 mm/year), High growth (≥0.40 mm/year).

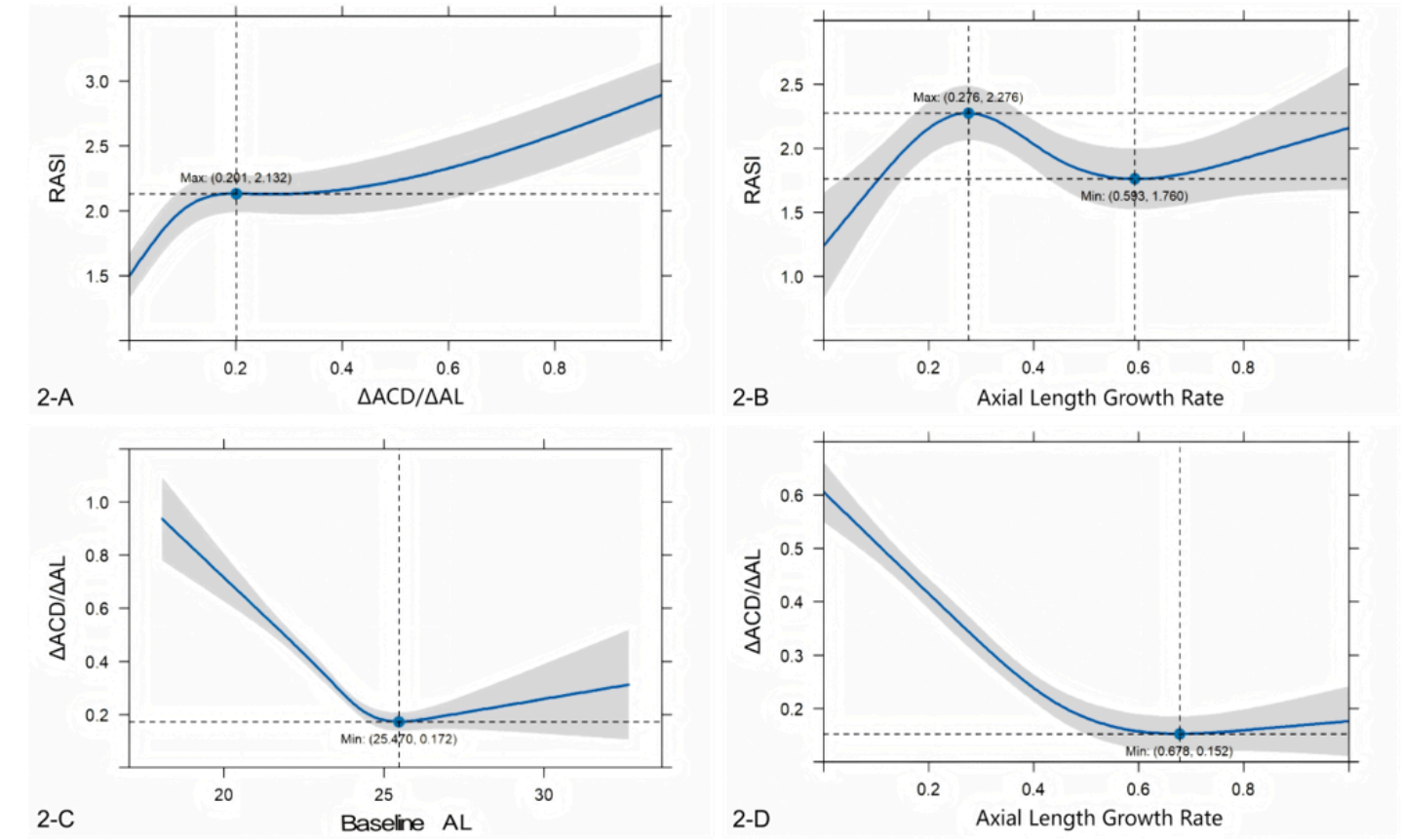


Figure 2

Restricted cubic spline analyses of nonlinear relationships between ocular biometric parameters.

(A) Nonlinear relationship between ΔACD/ΔAL and RASI. **(B)** Nonlinear relationship between axial length growth rate and RASI. **(C)** U-shaped relationship between baseline axial length and ΔACD/ΔAL. **(D)** Nonlinear relationship between axial length growth rate and ΔACD/ΔAL.

Abbreviations: RASI, Refractive Axial Sensitivity Index; ΔACD/ΔAL, ratio of anterior chamber depth change to axial length change; AL, axial length.

Note: Restricted cubic spline regression was performed with 4 knots placed at the 5th, 35th, 65th, and 95th percentiles of the predictor distribution. Solid blue lines represent the fitted spline curves; shaded gray areas indicate 95% confidence intervals. Dashed lines mark the locations of inflection points (maxima or minima), with coordinates displayed. All models were adjusted for age, sex, and baseline ocular biometric parameters.

Supplementary Files

This is a list of supplementary files associated with this preprint. Click to download.

- SupplementaryFigure.docx

- SupplementaryTables.docx
- Tables2and3.docx